

1 **The El Niño event of 2015-16: Climate anomalies and their impact on groundwater**
2 **resources in East and Southern Africa**

3

4 Seshagiri Rao Kolusu¹, Mohammad Shamsudduha^{2,3}, Martin C Todd¹, Richard G Taylor²,
5 David Seddon², Japhet J Kashaigili⁴, Girma Y Ebrahim⁵, Mark O Cuthbert^{2,6}, James P R
6 Sorensen⁷, Karen G Villholth⁵, Alan M MacDonald⁸, and Dave A MacLeod⁹

7

8 1. Department of Geography, University of Sussex, Brighton, BN1 9QS, UK

9 **Correspondence:**s.kolusu@sussex.ac.uk and sesukulusu@gmail.com

10 2. Department of Geography, University College London, Gower Street, London WC1E
11 6BT UK

12 3. Institute for Risk and Disaster Reduction, University College London, Gower Street,
13 London WC1E 6BT, UK

14 4. Sokoine University of Agriculture, Morogoro, Tanzania

15 5. International Water Management Institute, Pretoria, South Africa

16 6. School of Earth and Ocean Sciences, Cardiff University, Main Building, Park Place,
17 Cardiff, CF10 3AT, UK

18 7. British Geological Survey, Maclean Building, Crowmarsh Gifford, Wallingford,
19 Oxfordshire OX10 8BB UK

20 8. British Geological Survey, The Lyell Centre, Research Avenue South, Edinburgh
21 EH14 4AP UK

22 9. Atmospheric Oceanic and Planetary Physics, University of Oxford, OX1 3PU,UK

23

24 **Keywords**

25

26 El Nino; ENSO; Climate; groundwater; Africa; sustainability; recharge; climate impacts; water
27 management; GRACE

28

29 **Abstract**

30

31 The impact of climate variability on groundwater storage has received limited attention despite
32 widespread dependence on groundwater as a resource for drinking water, agriculture and
33 industry. Here, we assess the climate anomalies that occurred over Southern Africa (SA) and
34 East Africa, south of the equator (EASE), during the major El Niño event of 2015-16, and their
35 associated impacts on groundwater storage, across scales, through analysis of in situ
36 groundwater piezometry and GRACE satellite data. At the continental scale, the El Niño of
37 2015-16 was associated with a pronounced dipole of opposing rainfall anomalies over EASE
38 and Southern Africa, north/south of $\sim 12^{\circ}\text{S}$, a characteristic pattern of ENSO. Over Southern
39 Africa the most intense drought event in the historical record occurred, based on an analysis of
40 the cross-scale areal intensity of surface water balance anomalies (as represented by the
41 Standardised Precipitation-Evapotranspiration Index, SPEI), with an estimated return period of
42 at least 200 years and a best estimate of 260 years. Climate risks are changing and we estimate
43 that anthropogenic warming only (ignoring changes to other climate variables e.g.
44 precipitation) has approximately doubled the risk of such an extreme SPEI drought event.
45 These surface water balance deficits suppressed groundwater recharge, leading to a substantial
46 groundwater storage decline indicated by both GRACE satellite and piezometric data in the
47 Limpopo basin. Conversely, over EASE during the 2015-16 El Niño event, anomalously wet
48 conditions were observed with an estimated return period of ~ 10 years, likely moderated by
49 the absence of a strongly positive Indian Ocean Zonal Mode phase. The strong but not extreme
50 rainy season increased groundwater storage as shown by satellite GRACE data and rising
51 groundwater levels observed at a site in central Tanzania. We note substantial uncertainties in
52 separating groundwater from total water storage in GRACE data and show that consistency
53 between GRACE and piezometric estimates of groundwater storage is apparent when spatial
54 averaging scales are comparable. These results have implications for sustainable and climate-
55 resilient groundwater resource management, including the potential for adaptive strategies,
56 such as managed aquifer recharge during episodic recharge events.

57 **1. Introduction**

58

59 The El Niño-Southern Oscillation (ENSO) phenomenon is the dominant single driver of
60 interannual climate variability and large-scale extremes across the tropics including much of
61 Africa. Few studies have investigated the hydrological impacts of ENSO events on
62 groundwater. Here, we quantify climate anomalies and groundwater resources over Eastern
63 Africa, South of the Equator (EASE) and Southern Africa (SA), during the recent major El
64 Niño event of 2015-16, which in the Pacific sector was one of the strongest on record. El Niño
65 is typically associated with wet and dry anomalies over EASE and SA, respectively
66 (Ropelowski and Halpert, 1987), but with considerable diversity in this response among El
67 Niño events, in part related to the many other drivers of variability active over EASE and SA
68 (Supplementary Information S1). Much of SA experienced extreme drought in 2015-16 with
69 severe impacts on local food security, livelihoods and key sectors of the economy (SADC
70 2016a; 2016b; Archer *et al.*, 2017; Siderius *et al.*, 2018; Supplementary Information S1).

71

72 Groundwater is the dominant source of safe water for rural populations and many expanding
73 cities in EASE and SA (MacDonald *et al.*, 2012); in drylands, groundwater is often the only
74 perennial source of water. Although relatively under-developed to date, groundwater resources
75 are being developed rapidly in Africa (Taylor *et al.*, 2009; Calow *et al.*, 2010; Villholth *et al.*,
76 2013) and feature prominently in national development plans, especially to satisfy the need for
77 increased access to safe water and agricultural intensification under rapidly growing
78 populations and economic development. Groundwater is especially important in Africa where
79 surface runoff efficiency is lower than elsewhere (McMahon *et al.*, 1987) and drinking of
80 untreated surface water is associated with poor health (Hunter *et al.*, 2010). The long-term
81 viability of groundwater withdrawals and the livelihoods and ecosystems that groundwater
82 sustains depend on recharge.

83

84 Unlike surface water, research evaluating associations between groundwater storage and
85 ENSO, or indeed other modes of climate variability is rather limited (e.g. Holman *et al.*, 2011,
86 Kuss and Gurdak, 2014), despite evidence that climate variability and extreme rainfall
87 preferentially drive or restrict groundwater recharge. Several studies have shown recharge to
88 be episodic in semi-arid regions of Africa (Meyer *et al.*, 2005, van Wyk *et al.*, 2011, Taylor *et*

89 *al.*, 2013, Cuthbert *et al.*, 2017) and elsewhere (Jasechko and Taylor, 2015, Cuthbert *et al.*,
90 2016), highlighting the need to understand patterns and drivers of climate variability both
91 temporally and spatially, that influence recharge. Bonsor *et al.* (2018) analysed recent (2002-
92 2016) trends in, and seasonality of groundwater storage within 12 African sedimentary basins
93 implied from GRACE satellite data. Here, we employ evidence from both in situ observations
94 (piezometry) and GRACE satellite data to examine the effect of large-scale interannual climate
95 anomalies on groundwater across spatial scales for locations and domains that represent the
96 rainfall anomaly gradient over EASE and SA associated with characteristic El Niño response,
97 exemplified by the event of 2015-16. Beyond a few site-specific studies, the impacts of larger-
98 scale climate extremes on groundwater remain substantially unresolved. This hinders our
99 ability to determine acceptable levels of groundwater abstraction and depletion. This study
100 aims to quantify and understand the responses, during the 2015-16 El Niño of (i) the
101 surface/terrestrial water balance and (ii) groundwater storage over EASE and SA from regional
102 to local scales. Further, it seeks to place the 2015-16 El Niño event statistically in the historical
103 context.

104

105 **2. Data and methods**

106

107 2.1. Climate data and analysis

108

109 We analyse data over the broad region of Africa South of the Equator and over an extended
110 austral summer wet season of October-April, which encompasses the full wet season over SA
111 (excluding the Cape region) and those parts of EASE (south of $\sim 5^{\circ}\text{S}$), which experience a
112 similarly annual unimodal rainfall regime (Dunning *et al.*, 2016), and will accommodate the
113 response time of groundwater systems to climate. This region also experiences a coherent
114 ENSO signal (Section 3.1).

115

116 We use the Standardized Precipitation Evapotranspiration Index (SPEI) (Vicente-Serrano *et al.*
117 *al.*, 2010), which is a simple representation of surface water balance anomalies, derived over
118 this 7-month season (SPEI-7), over the period 1901 to present using precipitation data from the
119 Global Precipitation Climatology Centre (GPCC) monthly product v7 (Schneider *et al.*, 2011;
120 2014) at 1.0° resolution. To account for uncertainty in estimation of PET we use three

121 parameterisations of varying complexity: The Penman-Monteith equation, based on net
122 radiation, temperature, wind-speed and vapour pressure); The Hargreaves equation, based on
123 mean, minimum and maximum temperature and extra-terrestrial solar radiation; The
124 Thornthwaite equation, which is based solely on surface air temperature. The variables required
125 for the various PET estimates are obtained from the CRUTS3.24.01 dataset (Harris *et al.*,
126 2014). Note that some findings will be sensitive to this choice of drought index.

127

128 SPEI-7 anomalies are analysed for two large sub-domains, specifically EASE (4-12°S, 30-
129 40°E) and SA (10-35°S, 10-40°E) which encompass the anomalous wet and dry dipole
130 conditions, respectively, typically experienced during El Niño events (Fig. S1(b)) and
131 specifically in 2015-16 (Fig. 1(a)). For each domain, the areal extent and intensity of SPEI-7
132 in each year of the record was characterised using Intensity-Areal-extent Frequency (IAF)
133 curves of Mishra and Cherkauer (2010). IAF curves show the mean SPEI-7 value of grid cells
134 lying within various areal extent intervals: The areas covered by the lowest (for SA) or highest
135 (for EASE) 5th, 10th, 20th...100th areal percentiles of SPEI-7 grid cell values within the
136 domain area i.e. when all grid cells are ranked. The SPEI-7 IAF curves allow comparison
137 between years, irrespective of the precise spatial location of dry/wet anomalies within the
138 domain. This comparison includes estimating the return period of the SPEI-7 IAF curve
139 observed during the 2015-16 El Niño and other El Niño events. This is achieved by comparing
140 these observed SPEI-7 IAF curves to curves representing various benchmark return periods,
141 derived using a block maximum method applied to SPEI-7 data from a large ensemble of
142 climate model runs (see Supplementary Information S2).

143

144 It is likely that anthropogenic climate change is, and will continue to, affect large-scale
145 hydrology (Bindoff *et al.*, 2013). Here we estimate the effects purely of anthropogenic
146 temperature trends on drought risk over SA through a simplified attribution experiment. The
147 SPEI-7 IAF return period analysis above is repeated, but with respect to benchmark return
148 period IAF curves for which the temperature data, used in calculating PET, has the signal of
149 anthropogenic climate change removed (see Supplementary Information S2). As such, the
150 return period of the SPEI-7 IAF curve for 2015-16 is estimated in the context of the ‘real
151 historical’ world and for comparison in the context of a counterfactual climate with only natural
152 variability in temperature.

153

154 There is evidence to indicate recharge is preferentially driven by intense rainfall (see references
155 in Sections 1 and 3.1.1). To examine the nature of rainfall intensities over EASE during the El
156 Niño 2015-16 event we derive percentiles of the daily rainfall probability distribution from the
157 Tropical Rainfall Monitoring Mission (TRMM) 3B42 product during the (October-April
158 season, 1997-2016). In the absence of robust knowledge of actual rainfall thresholds associated
159 with groundwater recharge, and the likelihood that such thresholds are highly variable in space
160 and time, we derive the 80th percentile of daily rainfall within the season, at each grid cell as a
161 coarse proxy for rainfall events likely to be associated with recharge. Our results (Section 3.1.1)
162 are largely insensitive to the choice of percentile value (not shown). We derived the value of
163 the 80th percentile from all the (October-April) data and then just for the 2015-16 season and
164 show the anomalies. Finally, Information on the large-scale atmospheric circulation is
165 diagnosed from the horizontal and vertical winds, and specific humidity from ERA-Interim
166 reanalysis data (Dee *et al.*, 2011). SST data are obtained from the extended reconstructed sea
167 surface temperature (ERSST) version 4 from the National Oceanographic and Atmospheric
168 Administration (NOAA) (Smith *et al.*, 2008) on a 2° grid.

169

170 2.2 Groundwater storage estimates from GRACE satellite data

171

172 Regional-scale changes in groundwater storage (GWS) (2002-16) are estimated from GRACE
173 satellite measurements of total terrestrial water storage (TWS) anomalies, by subtracting
174 changes in the other terrestrial stores, which, in our tropical region, comprise soil moisture
175 (SMS) and surface water (SWS) stores (eq.1), themselves estimated from Land-Surface Model
176 (LSM) simulations, in the absence of in situ Δ SMS and Δ SWS data in the study areas.

177

$$178 \quad \Delta\text{GWS} = \Delta\text{TWS} - (\Delta\text{SMS} + \Delta\text{SWS}) \quad (\text{eq. 1})$$

179 Where Δ refers to the anomaly with respect to the long-term data series. To help interpretation
180 of the mean Δ GWS signals we also present the total uncertainty in estimates of Δ GWS, which
181 results from the uncertainty in estimates of Δ TWS, Δ SMS and Δ SWS. Regarding uncertainty
182 in Δ TWS associated with different GRACE processing strategies, we apply an ensemble mean
183 of three GRACE Δ TWS estimates. Namely, the CSR land (version RL05.DSTvSCS1409,
184 Swenson and Wahr, 2006; Landerer and Swenson, 2012) and JPL Global Mascon (version

185 RL05M_1.MSCNv01, Watkins *et al.*, 2015; Wiese *et al.*, 2015) solutions, from NASA's
186 *GRCTellus* data dissemination site (<http://grace.jpl.nasa.gov/data>), and a third GRGS GRACE
187 solution (CNES/GRGS release RL03-v1) (Biancale *et al.*, 2006) from the French Government
188 space agency, Centre National D'études Spatiales (CNES). Further information on the
189 processing involved in each product is provided in Supplementary Information S3. The
190 monthly GRACE Δ TWS are interpolated to a 1-degree grid for analysis in Equation 1. For
191 analysis of GRACE Δ TWS data at the locations of the two groundwater-level monitoring sites
192 of interest (Makutapora and Limpopo, see below) the monthly Δ TWS time-series are generated
193 by averaging over a 200 km radial buffer (i.e. area equivalent of $\sim 120\,000\text{ km}^2$) around each
194 location.

195
196 Further, to account for uncertainty in Δ SMS and Δ SWS we use data from four LSMs within
197 NASA's Global Land Data Assimilation System (GLDAS), and provide the associated
198 uncertainty ranges for each term. GLDAS is an uncoupled land surface modelling system that
199 includes multiple global LSMs driven by surface meteorology from the NCEP data assimilation
200 system, CMAP disaggregated precipitation and the Air Force Weather Agency satellite-derived
201 radiation fields (Rodell *et al.*, 2004). The four GLDAS LSMs are: The Community Land Model
202 (CLM, version 2) (Dai *et al.*, 2003), NOAH (version 2.7.1) (Ek *et al.*, 2003), the Variable
203 Infiltration Capacity (VIC) model (version 1.0) (Liang *et al.*, 2003), and MOSAIC Mosaic
204 (version 1.0) (Koster and Suarez, 1992). Further discussion of the uncertainty in these
205 individual water balance components (Fig. S2) and further information on the LSMs is
206 provided in Supplementary Information S3.

207

208

209 2.3 Groundwater storage estimates from piezometric observations

210

211 Groundwater-level time series records were compiled in two areas situated at the heart of the
212 EASE/SA ENSO rainfall dipole centres of action (Fig. 1(a)). (i) The Makutapora wellfield
213 (35.75°E , 5.90°S) site in central Tanzania, East Africa. Groundwater records were collated
214 from the Ministry of Water and Irrigation and the Dodoma Urban Water Supply, Tanzania.
215 Here, groundwater is abstracted from an aquifer comprising deeply weathered granite overlain
216 by alluvium (Taylor *et al.*, 2013). Data from three sites in the wellfield met the data quality

217 criteria and are averaged together; mean groundwater-level time series records were converted
218 to monthly anomalies in GWS using an in-situ derived specific yield (S_y) value of 0.06 (Taylor
219 *et al.*, 2013). We estimate that these data are representative of groundwater levels across an
220 area of $\sim 60 \text{ km}^2$. (ii) Limpopo Basin in Southern Africa (~ 28 to 32°E , 22.5 to 25°S).
221 Groundwater-level records from 40 stations within weathered hard-rock (“basement”) aquifers
222 in sub-basins A6 (Mogalakwena), A7 (Sand), A8 (Nzhelele) and A9 (Luvuvhu) of the Limpopo
223 Basin were collated from the Department of Water and Sanitation, Directorate Surface and
224 Groundwater Information, South Africa. The data were first standardised then averaged
225 together and represent an area estimated to be $\sim 47\,000 \text{ km}^2$. For both sites daily to monthly
226 groundwater-level records within our common study period of August 2002 to July 2016, were
227 checked for consistency (missing data less than 10%) and selected for groundwater storage
228 analysis. Mean groundwater-level time series records were converted to monthly anomalies in
229 GWS using a S_y value that produced the lowest root-mean square error between in situ and
230 GRACE GWS; the applied value (0.025) is consistent with that estimated for basement aquifers
231 in Africa by MacDonald *et al.* (2012).

232

233 We acknowledge that our estimates of GWS from piezometry may be influenced by
234 abstractions and we provide data on pumping rates from Makutapora (Fig. 5(c)). A numerical
235 method to remove the effects of pumping is currently the subject of ongoing research by the
236 authors, so in this case we infer the effect of pumping on GWS only in only relative qualitative
237 terms. Equivalent direct data on direct pumping rates is not available at Limpopo. However,
238 we note that Cai *et al.* (2017) mapped the spatial extent of irrigation across the Limpopo basin
239 in South African using satellite data and estimated that irrigation from groundwater provides
240 about 50% of the irrigated areas over 2% of the land area, which likely influences groundwater
241 storage locally.

242

243 **3. Results and discussion**

244

245 3.1 Climate anomalies over EASE and SA during the 2015-16 El Niño event

246

247 *3.1.1 EASE/SA climate anomalies*

248

249 The 2015-16 El Niño was the second strongest event within the available ~165-year Pacific
250 Ocean Sea Surface Temperature (SST) record, with SST anomalies exceeding 2°C for 6 months
251 from October 2015 (Fig. S1(d)). By some measures 2015-16 was the strongest El Niño since
252 1950 (Supplementary Information S1). Many of the observed climate anomalies around the
253 world were typical of El Niño years (Blunden and Arndt 2016). Over our study region, a
254 pronounced north-south dipole in SPEI-7 anomalies was observed (Fig. 1(a)), indicating
255 intense and extensive drought over SA (negative SPEI-7) and the wetter than normal conditions
256 over EASE (positive SPEI-7). In detail, most of SA south of 10°S experienced a substantial
257 water balance deficit: exceptional drought (SPEI <-2) conditions were experienced over
258 extensive parts of northern South Africa and northern Namibia, southern Botswana and
259 Zambia, as well as most of Zimbabwe and southern Mozambique and Malawi (Fig. 1(a)). Most
260 of EASE experienced above average rainfall during this period, with SPEI values >1 across
261 most of Tanzania, and a localised exceptionally wet region over the northernmost part of
262 Mozambique. The Makutapora and Limpopo sites (Fig. 1(a)) are located in areas representative
263 of the large-scale north/south rainfall dipole.

264

265 This spatial dipole pattern is very similar to the characteristic pattern of anomalies during El
266 Niño across the region, as represented by the leading Empirical Orthogonal Function (EOF) of
267 interannual variability (Fig. S1(b), Section S1) which correlates strongly with ENSO and
268 Indian Ocean SSTs Fig. S1(c). Indeed, the EOF coefficient value for 2015-16 is the second
269 highest within the entire 1901-2016 period. As such, across our study region 2015-16
270 represents an extreme exemplar of the characteristic El Niño climate response. Of course, a
271 complex set of planetary, regional and local scale processes related to, and independent of, El
272 Niño are fully responsible for the observed anomalies (e.g. Blamey *et al.*, 2018). The structure
273 of the atmospheric anomalies, specifically the mean meridional overturning circulation
274 associated with the large-scale SPEI-7 anomalies (Fig. 2(a)) shows large-scale anomalous
275 ascent over EASE between ~0° and 10°S indicative of enhanced deep convection, with
276 compensating descent over SA throughout the depth of the troposphere, which acts to suppress
277 convection. The low-level horizontal circulation (Fig. 2(b)) indicates key features associated
278 with the SPEI-7 dipole, notably: (i) An anomalous southerly flow from the southern Indian
279 Ocean into continental SA (Feature A in Fig. 2(b)), which weakens the transport of water
280 vapour from the humid tropical Indian Ocean leading to a decrease in moisture flux

281 convergence over SA. This is associated with a weakening of the mean ‘Mascarene’ subtropical
282 high over the Southern Indian Ocean (Feature B in Fig. 2(b)). (ii) Over EASE there are
283 anomalous low-level westerlies over Tanzania (Feature C in Fig. 2(b)), which weaken the mean
284 easterlies and enhance convergence over Tanzania, a structure characteristic of wet spells
285 (Berhane and Zaitchik, 2014; Nicholson 2017).

286

287 Groundwater recharge in the semi-arid tropics is favoured by high intensity rainfall events
288 (Owor, 2009; Jasechko and Taylor, 2015) within wet seasons, which may be modulated by
289 climate anomalies during El Niño conditions. During 2015-16, the intensities of the 80th
290 percentile of daily rainfall, a simple proxy of potential groundwater recharge-relevant rainfall,
291 increased by $\sim 1\text{-}5 \text{ mm day}^{-1}$ across much of EASE (Fig. 1(b)), representing a 100-150%
292 increase in many places. Whilst the association of rainfall intensity and enhanced recharge
293 across large and heterogeneous regions remains to be resolved, this intensification of rainfall
294 is consistent with greater groundwater recharge. Across SA the magnitude of the 80th
295 percentile reduced by $\sim 1\text{-}2 \text{ mm day}^{-1}$, potentially reducing groundwater recharge.

296

297 *3.1.2. The 2015-16 event in the historical context*

298

299 SPEI-7 IAF curves represent water balance anomalies across all spatial scales. For the SA
300 region, 2015/16 experienced the most extreme SPEI-7 drought within the historical period,
301 with an estimated IAF curve return period of ~ 260 years (range 190-290 years) (Fig. 3(a)). The
302 2015-16 drought was of greater intensity than those during previous El Niño events of
303 comparable magnitude, 1997-98 and 1982-83, whose SPEI-7 IAF curve return periods are
304 estimated to be only ~ 6 years (range 4-9 years) and ~ 43 years (range 35-47 years),
305 respectively). The contrasting intensity of SA drought between these events highlights the
306 diversity in responses over EASE/SA to El Niño, related to both the different character of the
307 events in the Pacific sector (2015-16 was strongest in the central rather than East Pacific as in
308 1997-98, see Section S1), and the specific regional circulation features during these events
309 which modulate the diverse ENSO teleconnections to SA (Ratnam *et al.*, 2014; Blamey *et al.*,
310 2018). Moreover, the 2015-16 drought followed a moderate drought in 2014-15 (Blamey *et al.*,
311 2018), which had important implications for groundwater levels (Section 3.2.2), and
312 statistically this 2-year drought event is remarkably unlikely. The extreme SPEI-7 anomalies

313 over SA in 2015-16 result from low rainfall and extremely high temperatures (Brundel and
314 Arndt, 2016, Russo *et al.*, 2016), potentially related to land-atmosphere feedback processes
315 (e.g. Seneviratne *et al.*, 2010), through reduced vegetation and soil moisture, perhaps persisting
316 from 2014-15. Uncertainty in the strength of land-atmosphere coupling over SA remains high
317 with contradictory results from model analyses (e.g. Koster *et al.*, 2006) and combined
318 observation-model analysis (Ferguson *et al.*, 2012), suggesting weak and strong coupling,
319 respectively. Further, warming across SA in recent decades can be attributed substantially to
320 anthropogenic radiative forcing (Bindoff *et al.*, 2013). As such climate risks are changing. We
321 estimate that the risk of a 2015-16 magnitude SPEI-7 drought over SA to have increased by
322 approximately two times due to the effects purely of anthropogenic warming. Note this
323 estimate does not include any anthropogenic changes in any of the other climate variables
324 which determine SPEI, most notably precipitation, nor changes in variability of climate (see
325 Supplementary Information S2). Further, other drought indices may have differing sensitivities
326 to anthropogenic temperature trends.

327

328 Over the EASE domain as a whole, the 2015-16 event was wet but not extreme, with an SPEI-
329 7 IAF curve estimated return period (Fig. 3(b)) of only ~10 years (range 5-12 years). The
330 anomalies were far weaker than that during the 1997-98 El Niño (Fig. 3b). These differences
331 may be associated with the state of the Indian Ocean Zonal Model (IOZM), an east-west
332 structure of coupled ocean-atmosphere circulation, influencing convection and rainfall over
333 East Africa (Saji *et al.*, 1999, Supplementary Information S1). The 1997-98 El Niño coincided
334 with a very strong positive IOZM event, unlike that of 2015-16, in which the IOZM was weakly
335 positive. Indeed, the wettest EASE year on record, 1961-1962, experienced a very strongly
336 positive IOZM event but no El Niño event (Nicholson, 2015).

337

338 3.2 Impact of 2015-16 climate anomalies on groundwater storage

339

340 *3.2.1 Large-scale estimates of ΔTWS , ΔSMS , ΔSWS and ΔGWS*

341

342 Regionally, GRACE ensemble-mean ΔTWS anomalies (Fig. 4(a)), and estimated ΔGWS (eq.
343 1, Fig. 4(d)), for 2015-16 reflect the north-south dipole over EASE/SA associated with the El
344 Niño-related SPEI-7 climate anomalies (Fig. 1(a)). Positive ΔTWS and ΔGWS anomalies exist

345 north of $\sim 10^{\circ}\text{S}$ across EASE (including the Makutapora site), the central DRC and northern
346 Angola. Negative ΔTWS and ΔGWS anomalies occur over an extensive region of eastern SA
347 including the Limpopo site. However, despite broad-scale structural similarity, there are some
348 apparent inconsistencies between ΔTWS (and other components of the water budget, including
349 ΔGWS) and the SPEI-7 climate signal that we consider below.

350

351 Viewed more closely, the partitioning of large-scale ΔTWS anomalies between the modelled
352 ΔSMS , ΔSWS and residual ΔGWS is spatially complex. First, we note that ΔSWS (Fig. 4(c))
353 plays only a minor role across the domain. Further, the coherence of the spatial structure in
354 anomalies in ΔSMS (Fig. 4(b)) is much less clear than for ΔTWS , reflecting uncertainties in
355 soil moisture among individual LSMs, as highlighted by Scanlon *et al.* (2018). Then,
356 considering the drought region over SA, a number of features emerge. (i) The relative
357 magnitude of ΔTWS deficits over South Africa are less than those of the SPEI-7, compared to
358 the northern more humid parts of SA (compare Figs 4(a) and 1(a)). This difference may be
359 expected since ΔTWS is an absolute measure of water volume whereas SPEI-7 is a standardised
360 anomaly relative to climate, derived over a much longer time period from a different rainfall
361 data than that used in the GLDAS system. Consequently, these measures may be expected to
362 diverge across mean rainfall gradients. Further, SPEI-7 reflects potential rather than actual
363 evapotranspiration. (ii) Over the northern sector of Zambia, Zimbabwe and Malawi the strongly
364 negative ΔTWS anomaly is almost equally shared between modelled reductions in ΔSMS and
365 ΔGWS . (iii) To the south over South Africa however, the (rather weaker) ΔTWS deficits are
366 effectively accounted for by ΔSMS anomalies such that ΔGWS anomalies are actually close to
367 zero or indeed slightly positive. The Limpopo study site lies at a transition zone between
368 regions with apparently strongly reduced ΔGWS to the northeast and close to zero or slightly
369 positive ΔGWS to the southwest. As geology is broadly continuous across the region, the
370 transition is largely related to uncertainty in the estimation of modelled ΔSMS .

371

372 Further, considering the anomalous wet region over EASE to the north of $\sim 10^{\circ}\text{S}$, ΔGWS
373 broadly mirrors the structure of ΔTWS , but the detailed picture is complex. Over most of
374 Tanzania and Angola positive ΔTWS anomalies are largely partitioned into the ΔGWS rather
375 than ΔSMS , whereas over southern DRC the reverse is the case. Moreover, there are interesting
376 apparent contradictions between the climate SPEI-7 and GRACE ΔTWS data. Over Namibia

377 and southern Angola, negative SPEI-7 (Fig. 1(a) and Δ SMS, Fig. 4(b)) coincides with positive
378 Δ TWS anomalies (Fig. 4(a)) leading to very strong positive Δ GWS anomalies (Fig. 4(d)) that
379 are therefore inconsistent with climate anomalies from SPEI-7. Conversely, and more locally,
380 over northern Mozambique, a positive Δ SMS anomaly, resulting from the driving rainfall data
381 (see the SPEI-7 wet anomaly, Fig. 1(a)) is not reflected in a strong Δ TWS signal, which leaves
382 a counterintuitive, negative residual response in Δ GWS. As such, GRACE Δ GWS exhibits
383 inconsistent responses to both apparent anomalous dry and wet conditions. These are likely to
384 be a result of (i) limitations in observational precipitation data, (ii) uncertainties in GRACE
385 TWS retrievals (as well as unwanted artefacts from surface and tectonic deformation) (iii)
386 uncertainties in estimation the individual components of water storage from LSMs, and (iv)
387 differing timescales of response across the various data. Such issues have been noted and
388 assessed elsewhere (Hassan and Jin, 2016; Zhao *et al.*, 2017; Rodell *et al.*, 2018; Scanlon *et*
389 *al.*, 2018). Resolving these issues is challenging but recent studies have sought to constrain the
390 uncertainty in the modelled components of water storage through assimilation of GRACE TWS
391 into hydrological models (Khaki *et al.*, 2018; Schumacher *et al.*, 2018).

392

393 3.2.2 *In situ and GRACE-derived estimates of Δ GWS at the Makutapora and Limpopo Basins*

394

395 Piezometry for the two observatory sites and changes in GWS estimated from GRACE and
396 LSMs are shown in Fig. 5. First, we note that uncertainty in the mean GRACE Δ GWS estimate
397 (blue shading around blue line in Figs. 5(a) and 5(b)), whilst often large, is generally smaller
398 than the signals of inter-annual variability which are the main focus of our analysis. However,
399 variability in mean GRACE Δ GWS within recharge seasons is small relative to uncertainty,
400 such that we cannot confidently draw inferences at these timescales.

401

402 Specifically, at the SA Limpopo site, observed piezometry (Fig. 5(a)) shows an annual cycle
403 in GWS in most years with a ‘saw tooth’ pattern representing steady recessions in GWS during
404 the dry season from May to October followed by rapid increases typically starting in December
405 in response to the onset of the wet season to peak post-wet season in April (lagging peak rainfall
406 by ~1-2 months). GWS in 2015-16 is well below average with a seasonal but subdued GWS
407 rise delayed (until March) due to the highly anomalous early wet season drought. The GWS
408 rise in March-April following rains in March is the second smallest on record; only 2002-3 has

409 lower seasonal increase in GWS. The 2015-16 drought is preceded by negligible recharge in
410 the dry year of 2014-15 (Fig. 5(a)), such that GWS as of mid-2016 was lowest in the 14-year
411 record. As such, the major drought of 2015-16 compounded weak recharge in the previous year
412 to leave GWS at historically low levels. This may have been compounded by increased
413 abstractions during these dry years.

414

415 Comparison of piezometry and GRACE-derived GWS at Limpopo (Fig 5(a)) suggests a broad
416 correspondence when seasonally averaged, ($r = 0.62$, significant at the 0.01 probability level).
417 The prolonged decline over 2014-16 is observed in both GRACE and piezometry. When
418 averaged over all years, the mean annual cycle is similar in phase and magnitude (not shown).
419 As such, at least broad temporal averaging scales GRACE is corroborated by piezometry at the
420 Limpopo site, where the scales of spatial averaging are similar. However, within-seasons, the
421 uncertainty in GRACE Δ GWS leads to a much ‘noisier’ mean signal at Limpopo which cannot
422 resolve the annual ‘saw-tooth’ pattern (Fig. 5(a)): in GRACE Δ GWS individual years have a
423 rather variable annual cycle despite a clear cycle in rainfall. Notably, a strong rise in the
424 ensemble mean GRACE Δ GWS during early season 2015-16 is not corroborated by piezometry
425 or rainfall. This period coincides with the greatest uncertainty in GRACE Δ GWS among the
426 three GRACE products (see blue shading around ensemble mean GRACE estimates in Fig 5a).
427 There is some indication from Fig. S2, that during such periods of greatest Δ GWS uncertainty,
428 it is the uncertainty in GRACE Δ TWS that makes most important contribution, rather than
429 uncertainty in the GLDAS components. From the individual GRACE Δ TWS products (Fig.
430 S3) we note that the mean GRACE vs. piezometry Δ GWS discrepancies in late 2015 result
431 largely from the GRGS product, which shows a non-corroborated increase in Δ TWS.

432

433 At the EASE Makutapora site, observed piezometric-GWS (Fig. 5(b)) shows little regular inter-
434 annual variability, with long periods of GWS recessions e.g. 2002-6, 2012-16, interrupted by
435 irregular and infrequent GWS increases, in declining order of magnitude 2006-7, 2009-10 and
436 2015-16, all El Niño years. The wet conditions in 2015-16 produced a major recharge event
437 though observed piezometric responses are smaller than in 2006-7 and 2009-10, despite higher
438 rainfall (Fig. 5(b)). Under highly dynamic pumping regimes (Fig. 5(c)), GWS changes are only
439 a partial proxy for groundwater recharge; the sharp increase (~50%) in wellfield pumping in
440 May 2015 served to diminish the response in piezometric-GWS to the 2015-16 El Niño.

441 Overall, however, the findings are consistent with the analysis of Taylor *et al.* (2013) who note
442 highly episodic recharge at Makutapora over the period since the 1960s associated with years
443 of heavy rainfall. The 2015-16 El Niño event represents a major event driving GWS at the
444 Makutapora wellfield, despite moderate rainfall anomalies over EASE.

445

446 There is only a rather general association between GRACE and piezometric estimates of
447 groundwater storage variability at the Makutapora site. However, the episodic recharge events
448 in the piezometry data of 2006-7, 2009-10 and 2015-16 are matched quite well by the
449 magnitude of major GRACE increases in Δ GWS, although the second largest GRACE Δ GWS
450 increase occurs in 2014-15 with no response apparent in piezometry. Overall, the seasonal
451 correlation of GRACE Δ GWS and piezometric GWS of 0.51 is only moderate (significant at
452 the 0.05 probability level) but clearly reflects the low frequency multi-annual trends (at least
453 up to 2013) as well as interannual variability.

454

455 However, stark differences between GRACE and piezometry are apparent. In contrast to
456 piezometry, GRACE (Fig. 5(b)) shows increases in Δ GWS in most years (with lag of ~1 month
457 after the rainfall annual peak), suggesting recharge occurs annually. Further, GRACE Δ GWS
458 replicates the low frequency recessionary trend over the period 2002-07 but diverges
459 substantially from piezometric observations after 2012. Resolving these contradictions is
460 problematic but two likely explanations emerge: (i) incommensurate scales of observation from
461 piezometry (area ~60 km²) and GRACE (~200,000 km²); and (ii) errors in GRACE Δ GWS
462 resulting from inaccurate accounting of Δ SMS and Δ SWS, which leaves a residual artefact of
463 an annual positive Δ GWS signal, see Section 3.1, Shamsudduha *et al.* (2017) and Scanlon *et*
464 *al.* (2018). For the latter, such errors may not be adequately accounted for in the uncertainty
465 estimates in GRACE Δ GWS given, for example similarities in LSM design and driving data.
466 Indeed, at both the Limpopo and Makutapora sites, we note stronger correlations between
467 seasonal local rainfall and piezometric GWS than with GRACE Δ GWS (not shown). For the
468 former, more localised processes may dominate the piezometry record, perhaps including
469 recharge sensitivity to contributions from local ephemeral river flow and rainfall. Further, the
470 effects of local pumping strongly influence the piezometric record, obscuring recharge events
471 of low magnitude. Specifically, the period 2002-07 over which the data agree reflects a
472 widespread groundwater recession, following the anomalously high recharge during the El

473 Niño event of 1997-98 (Taylor *et al.*, 2013), whilst the recent accelerated recessionary trend
474 since 2012 reflects the effects of a rapid increase in abstraction, which has a more localised
475 effect apparent only in the piezometric observations. As such the piezometric record may only
476 show episodic recharge whilst GRACE may indicate annual and episodic recharge processes.

477

478 **4. Concluding Discussion**

479

480 We quantify the climate anomalies and groundwater response during the major El Niño event
481 of 2015-16, over Southern and Eastern Africa, south of the equator, across a range of spatial
482 scales from regional to local. Our analysis confirms that the event was associated with a
483 pronounced north/south dipole pattern of positive/negative rainfall and water balance
484 anomalies over EASE/SA, typical of the ENSO teleconnection to the region. It was the second
485 largest such dipole event on record since 1900. Considerable diversity nevertheless exists in
486 climate anomalies over Africa between El Niño events.

487

488 The response of the water balance including GWS to ENSO is marked. Over EASE, total
489 rainfall and daily intensities were higher than normal and we estimate the return period for the
490 SPEI-7 water balance metric, over the domain as a whole, to be ~10 years. Wet anomalies over
491 EASE were actually moderated by the occurrence of a rather weak IOZM event. Nevertheless,
492 the anomalously wet conditions led to strong groundwater recharge over the EASE domain as
493 evidenced from GRACE. At the Makutapora wellfield in Tanzania, 2015-16 the strong El
494 Niño-related rainfall acted to reverse a long-term decline in observed in-situ groundwater
495 storage associated with a rise in intensive pumping rates. Changes in GWS estimated from an
496 ensemble of GRACE and LSMs also reflect the occurrence of substantial groundwater recharge
497 in 2015-16 and indicate annual groundwater recharge across the region. Broadly, the analysis
498 reinforces the importance of large-scale climate events in driving episodic recharge, critical to
499 replenish heavily exploited aquifers.

500

501 Over SA, the 2015-16 El Niño was associated with extreme drought, the strongest within the
502 observed 116-year record, with an estimated return period of ~260 years, resulting from
503 exceptionally low rainfall and high temperatures. The drought resulted in groundwater storage
504 declines through most of the wet season at our Limpopo study site, with strongly reduced

505 recharge experienced, the second lowest on record. Furthermore, this followed a dry year 2014-
506 15 leading to two consecutive years of low recharge and the greatest recession on record.
507 Clearly, groundwater provides a valuable buffer for periods of reduced surface water
508 availability in drought conditions, although as our results at Limpopo show, consecutive dry
509 years lead to marked storage reduction. Climate projections suggest reduced early season
510 rainfall across much of SA (Lazenby *et al.* 2018) compounding rising temperatures, and the
511 implications of this for climate resilience require a better understanding of these impacts on
512 groundwater recharge as well as surface water resources.

513

514 GRACE data and LSM outputs are clearly useful in complementing in-situ data, but a number
515 of issues emerge. Although at the broadest scale the GRACE Δ GWS anomalies in 2015-16 are
516 consistent with rainfall anomalies, there are a number of apparent inconsistencies over quite
517 large areas. Resolving the underlying reasons for these is problematic, but likely candidates
518 include the effects of inadequate climate data over Southern Africa, influencing and
519 compounded by uncertainties in Δ SMS and Δ SWS estimates simulated by land surface models,
520 on which the estimation of GRACE Δ GWS depends. When averaged over comparable scales
521 at Limpopo GRACE and piezometry agree well, at least for seasonal averages. Comparison
522 with the local observations shows that GRACE GWS estimates are considerably noisier,
523 especially at Makutapora where the spatial averaging scale of in-situ data and GRACE differ
524 greatly. Local groundwater abstractions are apparent in the Makutapora record and very likely
525 at Limpopo. Our results suggest that further analysis of the robustness of GRACE estimates of
526 GWS is advisable and, as such, these estimates should be treated with considerable caution.

527

528 Our results highlight the potential for adaptive strategies, such as managed aquifer recharge,
529 for optimising the capture or storage of episodic recharge in East Africa during El Niño and/or
530 positive IOZM events, and by corollary over Southern Africa during La Niña events (given the
531 opposing dipole structure of ENSO-related rainfall anomalies across SA/EASE). Of course
532 other modes of climate variability driving rainfall extremes are also important. Such
533 interventions can enhance the positive role of groundwater in climate-resilient water and
534 drought management. Seasonal climate prediction may have a potential role to inform such
535 adaptive water management strategies. At Makutapora, managed aquifer recharge exploiting
536 El Niño and/or positive IOZM events may contribute to resilient urban water supply systems

537 for the city of Dodoma. Our findings strengthen the case for a greater understanding of the
538 drivers of rainfall extremes over Africa and their relationship with recharge processes under
539 past, current and future climates and at various temporal and spatial scales. Such knowledge is
540 crucial to inform water management policies and practices for sustainable and climate resilient
541 development in a region undergoing rapid development of groundwater resources.

542

543 **Competing Interests.** The authors confirm they have no competing interests

544

545 **Author contribution.** SK and MT conceived the paper. Data analysis was conducted by all
546 authors. MT and SK prepared the manuscript with contributions from all co-authors.

547

548 **Acknowledgements**

549

550 This project was supported by the following research grant awards, funded by the UK Natural
551 Environment Research Council (NERC) and Economic and Social Research Council (ESRC)
552 and the UK Department for International Development (DfID): (i) The Unlocking the Potential
553 of Groundwater for Poverty Alleviation (UpGro) consortium project ‘*GroFutures*’ Grant
554 numbers NE/M008207/1 and NE/M008932/1; see www.grofutures.org) (ii) The Future
555 Climate For Africa (FCFA) consortium project ‘UMFULA’ grant number NE/M020258 (see
556 www.futureclimateafrica.org) (iii) The Science for Humanitarian Emergencies And Resilience
557 (SHEAR) consortium project ‘ForPac’ Grant number NE/P000673/1 and NE/P000568/1 (see
558 www.forpac.org). Further contribution was received from the UK Engineering and Physical
559 Sciences Research Council (EPSRC) ‘Banking the Rain’ grant number 172313 under the
560 Global Challenges Research Fund (GCRF), and The Royal Society Leverhulme Senior
561 Fellowship to RT (Ref. LT170004). MOC is supported by a UK NERC Independent Research
562 Fellowship, grant number NE/P017819/1. *The Chronicles Consortium* (<https://www.un-igrac.org/special-project/chronicles-consortium>), which coordinates long-term groundwater in
563 situ observations was supported by the UK government under the UPGro programme. This
564 research used science gateway resources of the National Energy Research Scientific
565 Computing Center, a DOE Office of Science User Facility supported by the Office of Science
566 of the U.S. Department of Energy under Contract No. DE-AC02-05CH11231. The authors
567 would like to thank the Editor and reviewers for their constructive comments and suggestions
568 which led to substantial improvements in the manuscript.

571 **References**

572

573 Archer, E. R. M., Landman, W. A., Tadross, M. A., Malherbe, J., Weepener, H., Maluleke, P.,
574 & Marumbwa, F. M.: Understanding the evolution of the 2014–2016 summer rainfall seasons
575 in southern Africa: Key lessons, *Clim. Risk Manag.*, *16*, 22-28, 2017.

576

577 Biancale, R., Lemoine, J-M., Balmino, G., Loyer, S., Bruisma, S., Perosanz, .F, Marty, J-C.,
578 and Gégout, P.: 3 Years of Geoid Variations from GRACE and LAGEOS Data at 10-day
579 Intervals from July 2002 to March 2005, CNES/GRGS, 2006

580

581 Bindoff, N.L., P.A. Stott, K.M. AchutaRao, M.R. Allen, N. Gillett, D. Gutzler, K. Hansingo,
582 G. Hegerl, Y. Hu, S. Jain, I.I. Mokhov, J. Overland, J. Perlwitz, R. Sebbari and X. Zhang,:
583 Detection and Attribution of Climate Change: from Global to Regional. In: Climate Change
584 2013: The Physical Science Basis. Contribution of Working Group I to the Fifth Assessment
585 Report of the Intergovernmental Panel on Climate Change [Stocker, T.F., D. Qin, G.-K.
586 Plattner, M. Tignor, S.K. Allen, J. Boschung, A. Nauels, Y. Xia, V. Bex and P.M. Midgley
587 (eds.)]. Cambridge University Press, Cambridge, United Kingdom and New York, NY, USA,
588 2013.

589

590 Berhane, F., & Zaitchik, B: Modulation of daily precipitation over East Africa by the Madden–
591 Julian oscillation, *J. Climate*, *27*(15), 6016-6034, 2014.

592

593 Blamey, R. C., Kolusu, S. R., Mahlalela, P., Todd, M. C., & Reason, C. J. C: The role of
594 regional circulation features in regulating El Niño climate impacts over southern Africa: A
595 comparison of the 2015/2016 drought with previous events, *Int. Journal of Climatol.*,
596 <https://doi.org/10.1002/joc.5668>, 2018.

597

598 Blunden, J., & Arndt, D. S. : State of the Climate in 2016, *B. Amer. Met. Soc.*, *98*(8), Si-S280,
599 2016.

600

601 Bonsor, H., Shamsudduha, M., Marchant, B., MacDonald, A., & Taylor, R: Seasonal and
602 decadal groundwater changes in African sedimentary aquifers estimated using GRACE
603 products and LSMs, *Remote Sens.*, *10*(6), 904, 2018.

604 Cai, X., Magidi, J., Nhamo, L., & van Koppen, B.: *Mapping irrigated areas in the Limpopo*
605 *Province, South Africa*(Vol. 172),International Water Management Institute (IWMI Working
606 Paper 172), doi: 10.5337/2017.205, 2017.

607 Calow, R. C., MacDonald, A. M., Nicol, A. L., & Robins, N. S. : Ground water security and
608 drought in Africa: linking availability, access, and demand, *Groundwater*, *48*(2), 246-256,
609 2010.

610

611 Cuthbert, M. O., Acworth, R. I., Andersen, M. S., Larsen, J. R., McCallum, A. M., Rau, G. C.,
612 & Tellam, J. H.: Understanding and quantifying focused, indirect groundwater recharge from
613 ephemeral streams using water table fluctuations, *Water Resour. Res.*, *52*(2), 827-840,
614 doi:10.1002/2015WR017503, 2016.

615

616 Cuthbert, M. O., Gleeson, T., Reynolds, S. C., Bennett, M. R., Newton, A. C., McCormack, C.
617 J., & Ashley, G. M. : Modelling the role of groundwater hydro-refugia in East African hominin
618 evolution and dispersal, *Nature Com.*, *8*, 15696, 2017.

619

620 Dai, Y., Zeng, X., Dickinson, R. E., Baker, I., Bonan, G. B., Bosilovich, M. G., ... & Oleson,
621 K. W. :The common land model, *B. Amer. Met. Soc.*, *84*(8), 1013-1024, 2003.

622

623 Dee, D. P., Uppala, S. M., Simmons, A. J., Berrisford, P., Poli, P., Kobayashi, S., ... & Bechtold,
624 P.: The ERA-Interim reanalysis: Configuration and performance of the data assimilation
625 system, *Q. J. Roy. Meteor. Soc.*, *137*(656), 553-597, 2011.

626

627 Dunning, C. M., Black, E. C., & Allan, R. P. : The onset and cessation of seasonal rainfall over
628 Africa, *J. Geophys. Res.-Atmos.*, *121*(19), 2016.

629

630 Ek, M. B., Mitchell, K. E., Lin, Y., Rogers, E., Grunmann, P., Koren, V., ... & Tarpley, J. D.
631 :Implementation of Noah land surface model advances in the National Centers for

632 Environmental Prediction operational mesoscale Eta model, *J. Geophys. Res.-*
633 *Atmos.*, 108(D22), 2003.

634

635 Ferguson, C. R., Wood, E. F., & Vinukollu, R. K. : A global intercomparison of modeled and
636 observed land–atmosphere coupling, *J. Hydromet.*, 13(3), 749-784, 2012.

637

638 Harris, I. P. D. J., Jones, P. D., Osborn, T. J., & Lister, D. H. :Updated high-resolution grids of
639 monthly climatic observations–the CRU TS3. 10 Dataset, *Int. J. Climatol.*, 34(3), 623-642,
640 2014.

641

642 Hassan, A., & Jin, S.: Water storage changes and balances in Africa observed by GRACE and
643 hydrologic models, *Geo. Geody.*, 7 (1), 39-49. <https://doi.org/10.1016/j.geog.2016.03.002>,
644 2016

645

646

647 Holman, I. P., Rivas-Casado, M., Bloomfield, J. P., & Gurdak, J. J. : Identifying non-stationary
648 groundwater level response to North Atlantic ocean–atmosphere teleconnection patterns using
649 wavelet coherence, *Hydrogeol. Jour.*, 19(6), 1269, 2011.

650

651 Hunter, P. R., MacDonald, A. M., & Carter, R. C. : Water supply and health, *PLoS*
652 *Medicine*, 7(11), e1000361, <https://doi.org/10.1371/journal.pmed.1000361>, 2010.

653

654 Jasechko, S., & Taylor, R. G. : Intensive rainfall recharges tropical groundwaters. *Env.*
655 *Research Let.*, 10(12), 124015, doi:10.1088/1748-9326/10/12/124015, 2015.

656

657 Khaki, M., Forootan, E., Kuhn, M., Awange, J., van Dijk, A.I.J.M., Schumacher, M., & Sharifi,
658 M.A. Determining Water Storage Depletion within Iran by Assimilating GRACE data into the
659 W3RA Hydrological Model, *Adv. Water Resour.*, doi: 10.1016/j.advwatres.2018.02.008, 2018

660

661 Koster, R. D., & Suarez, M. J. :Modeling the land surface boundary in climate models as a
662 composite of independent vegetation stands, *J. Geophys. Res.-Atmos.*, , 97(D3), 2697-2715,
663 1992.

664

665 Koster, R. D., Sud, Y. C., Guo, Z., Dirmeyer, P. A., Bonan, G., Oleson, K. W., ... & Kowalczyk,
666 E. : GLACE: the global land-atmosphere coupling experiment. Part I: overview, *J.*
667 *Hydromet.*, 7(4), 590-610, 2006.

668

669 Kuss, A. J. M., & Gurdak, J. J. : Groundwater level response in US principal aquifers to ENSO,
670 NAO, PDO, and AMO, *J. Hydro.*, 519, 1939-1952, 2014.

671

672 Landerer, F. W., & Swenson, S. C. :Accuracy of scaled GRACE terrestrial water storage
673 estimates, *Water Resour. Res.*, 48(4), 2012.

674

675 Lazenby, M. J., Todd, M. C., & Wang, Y., Chadwick. R.:Future precipitation projections over
676 central and southern Africa and the adjacent Indian Ocean: What causes the changes and the
677 uncertainty? *J. Climate*, 31, 4807-4826, 2018

678

679 Liang, X., Xie, Z., & Huang, M. :A new parameterization for surface and groundwater
680 interactions and its impact on water budgets with the variable infiltration capacity (VIC) land
681 surface model, *J. Geophys. Res.-Atmos.*, 108(D16), 2003.

682

683 MacDonald, A. M., Bonsor, H. C., Dochartaigh, B. É. Ó., & Taylor, R. G. :Quantitative maps
684 of groundwater resources in Africa, *Env. Research Let.*, 7(2), 024009, 2012.

685

686 McMahon, T. A., Finlayson, B. L., Haines, A., & Srikanthan, R.: Runoff variability: a global
687 perspective, In *The Influence of Climate Change and Climatic Variability on the Hydrologic*
688 *Regime and Water Resources*, Proceedings of the Vancouver Symposium, August 1987. IAHS
689 Publ. no. 168, 1987.

690

691 Meyer, R.: Analysis of groundwater level time series and the relation to rainfall and recharge,
692 Water Resources Commission (South Africa), report number 1323/1/05, 2005.

693

694 Mishra, V., & Cherkauer, K. A.: Retrospective droughts in the crop growing season:
695 Implications to corn and soybean yield in the Midwestern United States, *Agr. Forest*
696 *Met.*, 150(7-8), 1030-1045, 2010.

697

698 Nicholson, S.E.: Long-term variability of the East African ‘short rains’ and its links to large-
699 scale factors, *Int. J. Climatol.*, 35(13), 3979-3990, 2015

700

701 Nicholson, S. E.: Climate and climatic variability of rainfall over eastern Africa, *Reviews of*
702 *Geophysics*, 55(3), 590-635, 2017.

703

704 Owor, M., Taylor, R. G., Tindimugaya, C., & Mwesigwa, D.: Rainfall intensity and
705 groundwater recharge: empirical evidence from the Upper Nile Basin, *Env. Research*
706 *Let.*, 4(3), 035009, 2009.

707

708 Ratnam, J. V., Behera, S. K., Masumoto, Y., & Yamagata, T. :Remote effects of El Niño and
709 Modoki events on the austral summer precipitation of southern Africa, *J. Climate*, 27(10),
710 3802-3815, 2014.

711

712 Rodell, M., Houser, P. R., Jambor, U. E. A., Gottschalck, J., Mitchell, K., Meng, C. J., ... &
713 Entin, J. K. ;The global land data assimilation system, *B. Am. Meteorol.*, 85(3), 381-394, 2004.

714

715 Rodell , M., Famiglietti, S., Wiese, D.N., Reager, J.T., Beaudoing, H. K., Landerer F. W.
716 & Lo, M.-H. : Emerging trends in global freshwater availability, *Nature*, 557, 651- 659.
717 <https://www.nature.com/articles/s41586-018-0123-1>, 2018

718

719 Ropelewski, C. F., & Halpert, M. S.: Global and regional scale precipitation patterns associated
720 with the El Niño/Southern Oscillation, *Mon. Weather Rev.*, 115(8), 1606-1626, 1987.

721

722 Russo, S., Marchese, A. F., Sillmann, J., & Immé, G.: When will unusual heat waves become
723 normal in a warming Africa?, *Env. Research Let.*, 11(5), 054016, 2016.

724

725 SADC 2016a: SADC regional situation update on El Nino-induced drought, Issue 02, 12th
726 September 2016, SADC, 12pp, available at:

727 ,https://www.sadc.int/files/9514/7403/9132/SADC_Regional_Situation_Update_No-2_16-
728 09-2016.pdf, 2016.

729

730 SADC 2016b: SADC Regional Vulnerability Assessment and Analysis Synthesis Report: State
731 of Food Insecurity and Vulnerability in the Southern African Development Community,
732 SADC, 66pp, available at: https://www.sadc.int/files/9014/7911/5767/SADC_RVAA-
733 [August-Final-Web.pdf](https://www.sadc.int/files/9014/7911/5767/SADC_RVAA-), 2016

734

735 Saji, N. H., Goswami, B. N., Vinayachandran, P. N., & Yamagata, T.: A dipole mode in the
736 tropical Indian Ocean, *Nature*, 401(6751), 360, doi:10.1038/43854, 1999.

737

738 Scanlon, B. R., Zhang, Z., Save, H., Sun, A. Y., Schmied, H. M., van Beek, L. P., ... &
739 Longuevergne, L. : Global models underestimate large decadal declining and rising water
740 storage trends relative to GRACE satellite data, *P. Natl. Acad. Sci.*, 201704665,
741 <https://doi.org/10.1073/pnas.1704665115>, 2018.

742

743 Schneider, U., Becker, A., Finger, P., Meyer-Christoffer, A., Rudolf, B., Markus, Z.: GPCC
744 Full Data Reanalysis Version 6.0 at 0.5°: Monthly Land-Surface Precipitation from Rain-
745 Gauges built on GTS-based and Historic Data. DOI: [10.5676/DWD_GPCC/FD_M_V6_100](https://doi.org/10.5676/DWD_GPCC/FD_M_V6_100),
746 [2011](https://doi.org/10.5676/DWD_GPCC/FD_M_V6_100).

747

748 Schneider, U., Becker, A., Finger, P., Meyer-Christoffer, A., Ziese, M., & Rudolf, B. : GPCC's
749 new land surface precipitation climatology based on quality-controlled in situ data and its role
750 in quantifying the global water cycle, *Theor. Appl. Climatol.*, 115(1-2), 15-40, 2014.

751

752 Schumacher, M., Forootan, E., van Dijk, A.I.J.M., Muller Schmied, H., Crosbie, R.S., Kusche,
753 855 J., & Dll, P. Improving drought simulations within the Murray-Darling Basin by 856
754 combined calibration/assimilation of GRACE data into the WaterGAP Global Hydrology 857
755 Model, *Remote Sens. Environ.*, 204, 212-228, <https://doi.org/10.1016/j.rse.2017.10.029>, 2018
756

757 Seneviratne, S. I., Corti, T., Davin, E. L., Hirschi, M., Jaeger, E. B., Lehner, I., ... & Teuling,
758 A. J.: Investigating soil moisture–climate interactions in a changing climate: A review, *Earth*
759 *Review.*, 99(3-4), 125-161, doi:10.1016/j.earscirev.2010.02.004, 2010.

760

761 Shamsudduha, M., Taylor, R. G., Jones, D., Longuevergne, L., Owor, M., & Tindimugaya, C.
762 :Recent changes in terrestrial water storage in the Upper Nile Basin: an evaluation of commonly
763 used gridded GRACE products, *Hydrol. Earth Syst. Sci.*, 21(9), 4533-4549,
764 <https://doi.org/10.5194/hess-21-4533-2017>, 2017.

765

766 Siderius, C., Gannon, K. E., Ndiyoi, M., Opere, A., Batisani, N., Olago, D., ... & Conway, D.
767 :Hydrological response and complex impact pathways of the 2015/2016 El Niño in Eastern and
768 Southern Africa, *Earth's Fut.*, 6(1), doi:10.1002/2017EF000680,2-22, 2018.

769

770 Smith, T. M., Reynolds, R. W., Peterson, T. C., & Lawrimore, J. : Improvements to NOAA's
771 historical merged land–ocean surface temperature analysis (1880–2006). *J. Climate*, 21(10),
772 2283-2296, 2008.

773

774 Swenson, S., & Wahr, J.: Post-processing removal of correlated errors in GRACE
775 data, *Geophys. Res. Lett.*, 33(8), 2006.

776

777 Taylor, R. G., Koussis, A. D., & Tindimugaya, C.: Groundwater and climate in Africa—a
778 review, *Hydro. Sci. Jour.*, 54(4), 655-664, 2009.

779

780 Taylor, R. G., Todd, M. C., Kongola, L., Maurice, L., Nahozya, E., Sanga, H., & MacDonald,
781 A. M. : Evidence of the dependence of groundwater resources on extreme rainfall in East
782 Africa, *Nature Clim. Chan.*, 3(4), 374, 2013.

783

784 van Wyk, E., Van Tonder, G. J., & Vermeulen, D.: Characteristics of local groundwater
785 recharge cycles in South African semi-arid hard rock terrains–rainwater input, *Water SA*, 37(2),
786 <http://dx.doi.org/10.4314/wsa.v37i2.65860>, 2011.

787

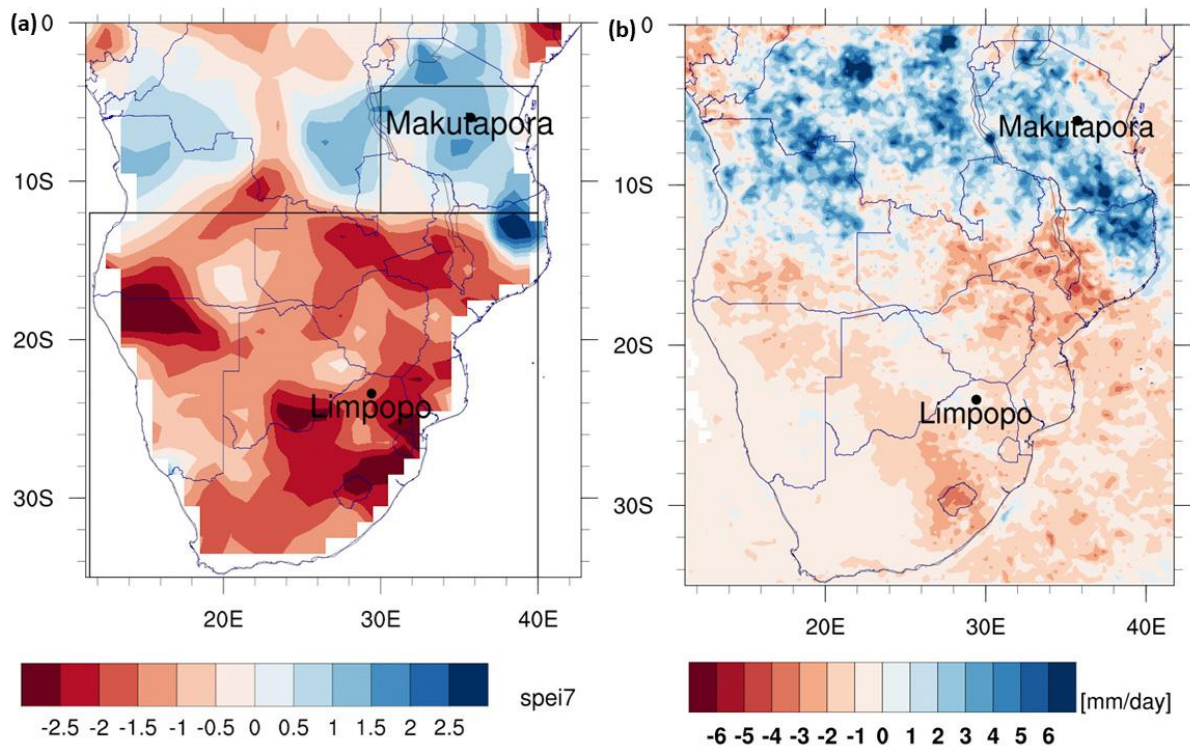
788 Vicente-Serrano, S. M., Beguería, S., & López-Moreno, J. I. : A multiscale drought index
789 sensitive to global warming: the standardized precipitation evapotranspiration index, *J.*
790 *Climate*, 23(7), 1696-1718, 2010.
791

792 Villholth, K. G. : Groundwater irrigation for smallholders in Sub-Saharan Africa—a synthesis
793 of current knowledge to guide sustainable outcomes, *Water intern.*, 38(4), 369-391, 2013.
794

795 Watkins, M. M., Wiese, D. N., Yuan, D. N., Boening, C., & Landerer, F. W. : Improved
796 methods for observing Earth's time variable mass distribution with GRACE using spherical cap
797 mascons, *J. Geo. Res.: Solid Earth*, 120(4), 2648-2671, 2015.
798

799 Wiese, D. N., Yuan, D-N., Boening, C., Landerer, F. W., & Watkins, M. M.: JPL GRACE
800 Mascon Ocean, Ice, and Hydrology Equivalent Water Height, JPL RL05M.1. Ver. 1 PO.DAAC
801 CA USA, 2015.
802

803 Zhao, M., Velicogna, G.A.I., & Kimball, J.S.: Satellite observations of regional drought
804 severity in the continental United States using GRACE-based terrestrial water storage changes,
805 *J. Climate*, 30, 6297-6308. DOI: 10.1175/JCLI-D-16-0458.1, 2017
806
807



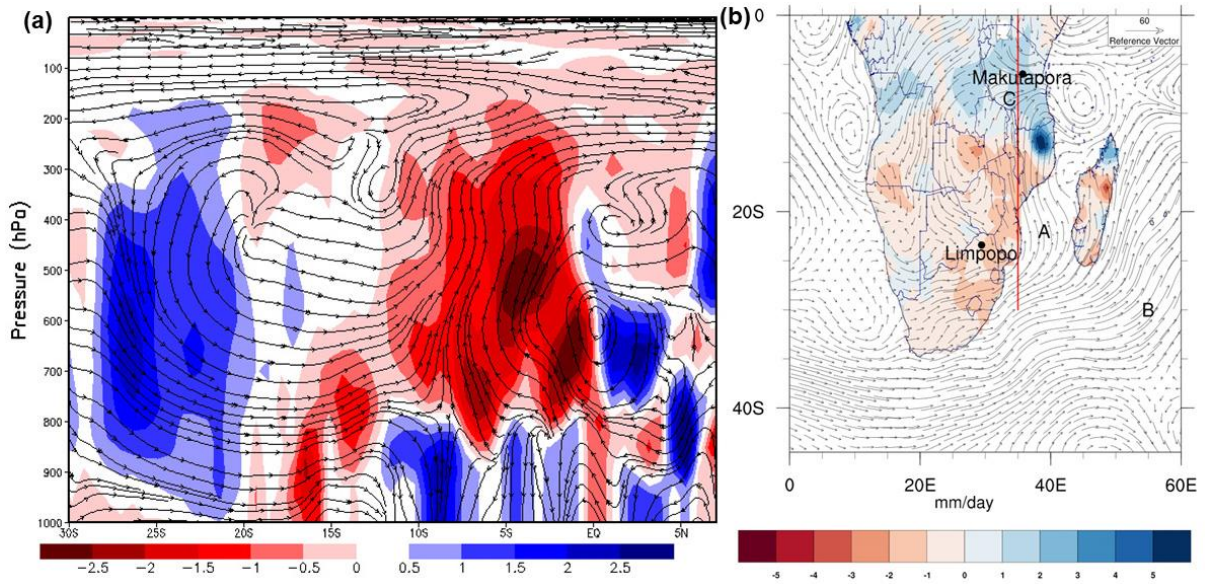
808

809

810 Fig. 1. Large-scale climate anomalies over the study region for October-April 2015-16. (a)
 811 SPEI-7 (b) Anomalies of the 80th percentile of daily TRMM rainfall (mm day^{-1}). Boxes in (a)
 812 show the EASE (small box) and SA (large box) domains used in the SPEI-7 IAF analysis (see
 813 Section 2.1 and S2). The piezometer observation locations are also shown.

814

815

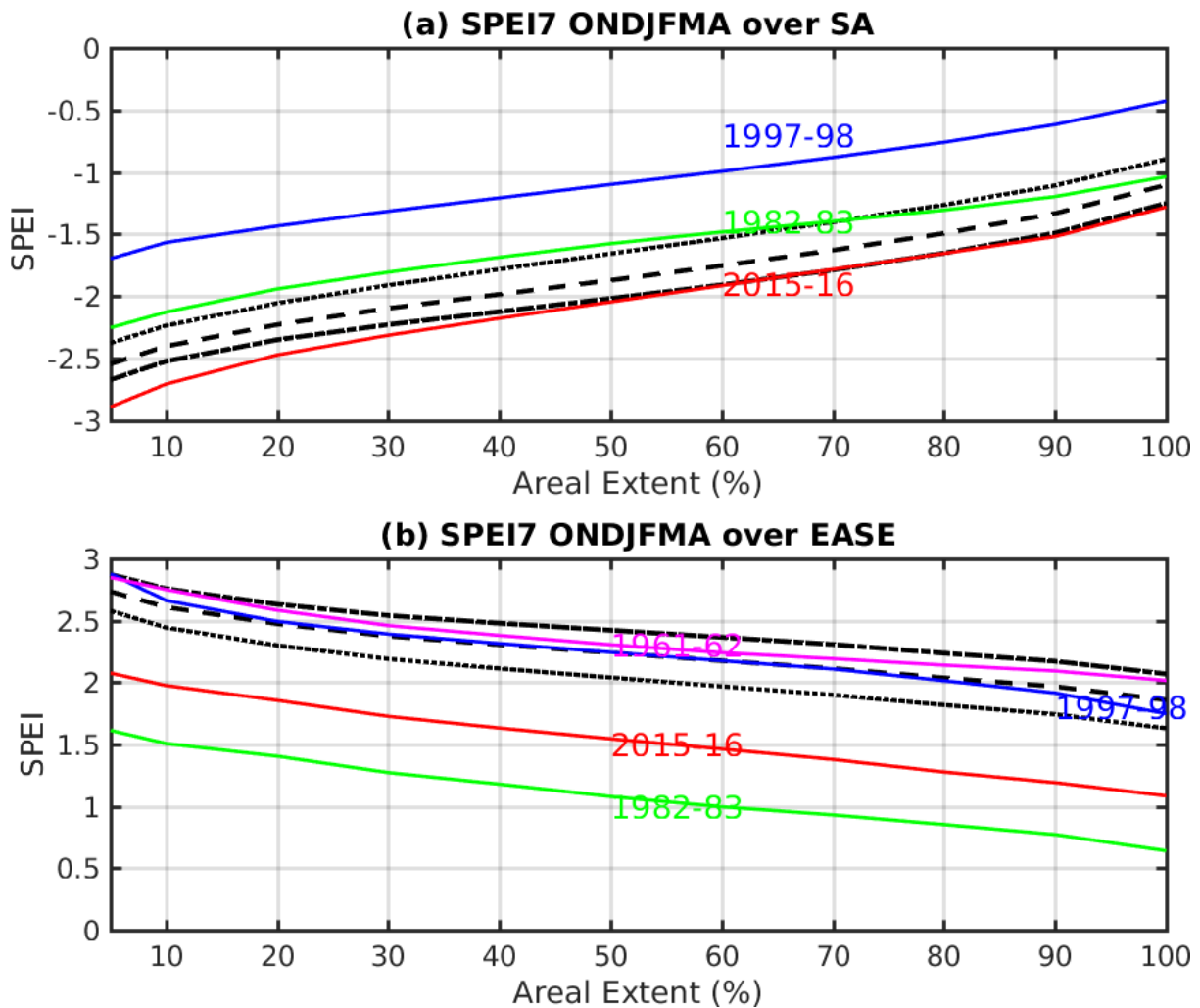


816

817

818

819 Fig. 2. Circulation anomalies for October-April 2015-2016. (a) Latitude-height transect plot of
 820 anomalous meridional overturning circulation (streamlines of vertical and meridional wind)
 821 and vertical velocity anomalies (m s^{-1} , shaded) averaged over the 35-37°E. This latitude transect
 822 is shown as a red line on the map in Fig. 2(b). (b) Vertically integrated moisture flux anomalies
 823 ($\text{g kg}^{-1} \text{m s}^{-2}$, vectors) and rainfall anomalies (mm day^{-1} , shaded).



824

825

826 Fig. 3. Intensity-Areal extent-Frequency (IAF) curves (See Section 2.1 and Section S2 for
 827 details of method) estimated from the seasonal mean SPEI-7 (derived with Penman-Monteith
 828 PET, see text for uncertainty ranges) over (a) the southern Africa domain (10.5° - 35.5° S, see
 829 box in Fig. 1a); (b) the east Africa domain 30° - 40° E, 4° - 12° S, see box in Fig. 1a). On the x-
 830 axis is the areal extent over which the SPEI is averaged and the y-axis is the SPEI-7 drought
 831 intensity. Solid coloured lines show the IAF curves for the study El Niño event years; 2015-16
 832 (red), 1997-98 (blue), 1982-83 (green) and (in (b) only) the 1961-62 Indian Ocean Zonal Mode
 833 event (purple). Black lines are the IAF curves for selected benchmark return periods, from top
 834 to bottom in (a) (and bottom to top in (b)), 50 years (dotted), 100 years (dashed) and 200 years
 835 (dot-dashed).

836
837
838
839
840
841
842
843
844
845
846
847
848
849
850
851
852
853
854
855
856
857
858
859
860
861
862
863
864
865

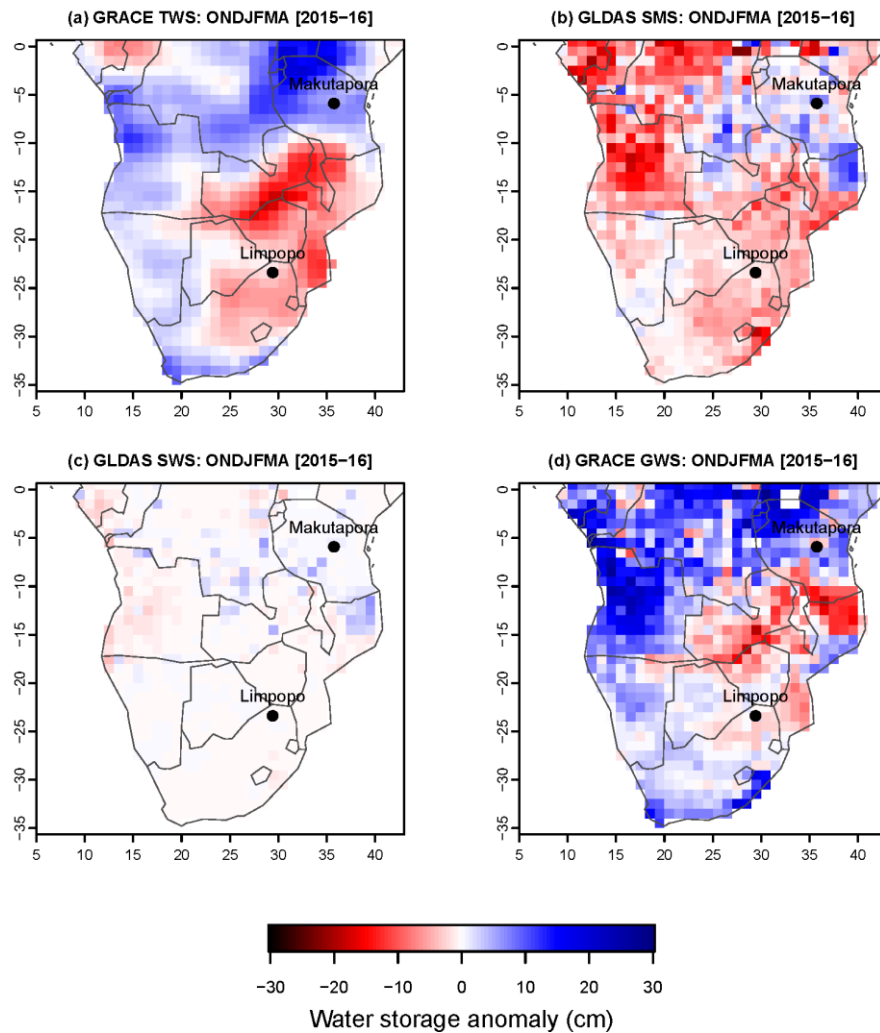
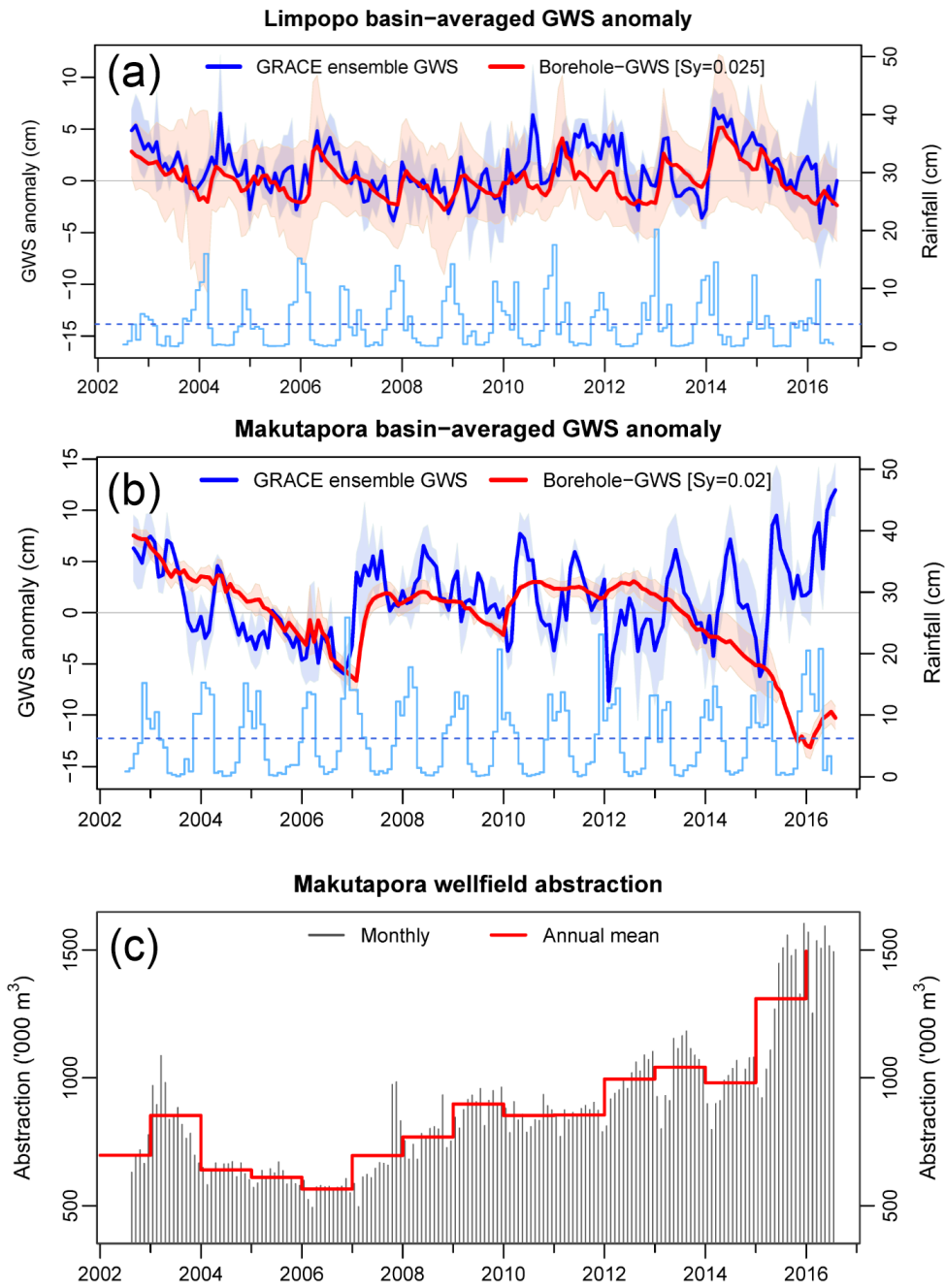


Fig. 4. Water storage anomaly components (cm) over the study domain for the wet season (October-April) of 2015-16 minus long term annual mean 2003-15. (a) GRACE ensemble mean total water storage anomaly (Δ TWS, from CSR, JPL-Mascons, GRGS GRACE products); (b) GLDAS ensemble mean soil moisture storage anomaly (Δ SMS, 4 land surface models: CLM, NOAH, VIC, MOSAIC); (c) GLDAS ensemble mean surface runoff or surface water storage anomaly (Δ SWS, from 4 land surface models: CLM, NOAH, VIC, MOSAIC); and (d) GRACE-GLDAS derived ensemble mean groundwater storage anomaly (Δ GWS, from 3 estimates of Δ GWS from 3 GRACE products).

866
 867
 868
 869
 870
 871
 872
 873
 874
 875
 876
 877
 878
 879
 880
 881
 882
 883
 884
 885
 886
 887
 888
 889
 890



891 Fig. 5. (a) Time series of estimates of monthly Δ GWS anomaly (cm) at Limpopo from August
 892 2002 to July 2016 derived from GRACE averaged over an area approximately $\sim 120\,000\text{ km}^2$
 893 (bold blue line is the mean of CSR, JPL-Mascons and GRGS products, light blue shading
 894 representing uncertainty across the three products and four LSMs) and piezometry (red line,
 895 mean of all stations, red shading represents uncertainty). Monthly rainfall (from GPCP product,
 896 cm) shown as bars with mean monthly rainfall indicated by a dashed line. (b) As (a) but for
 897 Makutapora. (c) Monthly groundwater abstraction at Makutapora.